Rational design of a Kv1.3 channel-blocking antibody as a selective immunosuppressant

Rongsheng E. Wang[a,b], Ying Wang[b], Yuhan Zhang[b], Chase Gabrelow[b], Yong Zhang[b], Victor Chi[b], Qiangwei Fu[b], Xiaozhou Luo[a], Danling Wang[b], Sean Joseph[b], Kristen Johnson[b], Arnab K. Chatterjee[b], Timothy M. Wright[b], Vân T. B. Nguyen-Tran[b], John Teijaro[c], Argyrios N. Theofilopoulos[c], Peter G. Schultz[a,b,1], and Feng Wang[b,1]

[a]Department of Chemistry and the Skaggs Institute for Chemical Biology, The Scripps Research Institute, La Jolla, CA 92037; [b]California Institute for Biomedical Research, La Jolla, CA 92037; and [c]Department of Immunology and Microbial Science, The Scripps Research Institute, La Jolla, CA 92037

A variable region fusion strategy was used to generate an immunosuppressive antibody based on a novel "stalk-knob" structural motif in the ultralong complementary-determining region (CDR) of a bovine antibody. The potent Kv1.3 channel inhibitory peptides Moka1-toxin and Vm24-toxin were grafted into different CDRs of the humanized antibodies BVK and Synagis (Syn) using both β-sheet and coiled-coil linkers. Structure-activity relationship efforts led to generation of the fusion protein Syn-Vm24-CDR3L, which demonstrated excellent selectivity and potency against effector human memory T cells (subnanomolar to picomolar EC$_{50}$ values). This fusion antibody also had significantly improved plasma half-life and serum stability in rodents compared with the parent Vm24 peptide. Finally, this fusion protein showed potent in vivo efficacy in the delayed type hypersensitivity in rats. These results illustrate the utility of antibody CDR fusions as a general and effective strategy to generate long-acting functional antibodies, and may lead to a selective immunosuppressive antibody for the treatment of autoimmune diseases.

antibody | protein engineering | Kv1.3 | autoimmune | immunosuppressive

Autoreactive memory T lymphocytes are believed to mediate the pathogenesis of autoimmune diseases, such as multiple sclerosis, type 1 diabetes mellitus, rheumatoid arthritis, inflammatory bowel disease, psoriasis, and lupus (1–9). Current therapeutics for autoimmune diseases and other T-cell–mediated inflammatory disorders are based on the general inhibition or depletion of T cells and other leukocytes (10–12). Nonselective immunosuppression by such drugs as corticosteroids, FK506, and cyclosporine often leads to severe side effects, including opportunistic infections (11, 13, 14). Therapeutics designed to specifically inhibit the function of effector memory T (T_{EM}) cells without impairing the function of naive T cells or central memory T (T_{CM}) cells may offer an improved safety profile for the treatment of autoimmune diseases and organ transplantation.

One therapeutic target that is the focus of considerable interest is the voltage-gated potassium channel Kv1.3, which, together with the calcium-activated K$^+$ channel KCa3.1, is required to mediate membrane potential and calcium signaling in T cells (15). T_{EM} cells have been observed to up-regulate Kv1.3 on activation with no change in KCa3.1 levels (1, 15). In contrast, naive T cells and T_{CM} cells up-regulate KCa3.1 after activation with little change in Kv1.3 expression (1, 15). Thus, inhibitors of Kv1.3 function are expected to specifically inhibit the activation of T_{EM} cells, and thereby selectively ameliorate T-cell–mediated inflammatory diseases without compromising normal immune responses (15).

The generation of small molecules or antibodies that potently and selectively block Kv1.3 activity has proven challenging (16). Although a number of peptide toxins with multiple disulfide bonds from spiders, scorpions, and anemones are known to block specific ion channels, including Kv1.3, only a few selective, potent peptide inhibitors of the Kv1.3 channel have been explored as potential therapeutics (17). Of these, the synthetic derivative of stichodactyla toxin (ShK) with an unnatural amino acid (ShK-186) is the most advanced. This peptide has demonstrated efficacy in preclinical

studies, has recently completed a phase I clinical trial for treatment of psoriasis (18), and is currently being evaluated clinically in multiple autoimmune diseases. However, small peptides like ShK-186 are rapidly cleared by the kidney after administration, resulting in short circulating half-lives (<10 min in rats) (17, 18), raising uncertainty as to the dosing frequency required for optimal clinical efficacy. Moreover, synthetic peptides with multiple disulfide bonds can prove difficult to fold and cross-link into the proper bioactive conformation, which may complicate commercial production. Thus, there is a compelling need for the development of long-acting, selective Kv1.3 inhibitors for the treatment of chronic inflammatory diseases.

We recently solved the X-ray crystal structure of bovine antibody BLV1H12 with an ultralong heavy-chain complementary-determining region (CDR)-3 (CDR3H) that folds into a unique structural motif (19). The solvent-exposed antiparallel β-strand stalk terminates in a disulfide cross-linked knob domain to afford a unique "stalk-knob" structure. Inspired by this discovery, we grafted a number of proteins and peptides into CDR3H to generate functional bovine antibody-CDR3H fusions (20–23). The stalk motif can be either an antiparallel β-strand or a heterodimeric coiled-coil to support the correct folding of the peptide/protein replacing the knob domain. The knob domain has been replaced with a number of different hormones, growth factors, and cytokines that retain their biological activity. The Ig scaffold provides

Significance

There is considerable interest in developing immunosuppressants that can specifically target effector memory T cells which are key to the pathogenesis of many inflammatory disorders. The potassium channel Kv1.3 has been found to play an important role in T_{EM} activation, but not in naive and central memory T cells. It has proven challenging to generate small molecules or antibodies that potently and selectively block Kv1.3 function. We generated antibody fusions by grafting potent Kv1.3 blocking peptides into complementary-determining regions (CDRs) of humanized antibodies, and among those, identified a candidate with high in vitro potency, excellent physicochemical and pharmacologic properties, and in vivo efficacy in a rat model. These novel toxin-antibody fusions have therapeutic potential for a variety of T_{EM}-mediated inflammatory diseases.

APPLIED BIOLOGICAL SCIENCES

a long serum half-life and ease of recombinant protein production. In addition, we have shown that the bovine Ig scaffold can be substituted with human Ig scaffolds (24–27). Given that the diversity of disulfide patterns in the knob domain is similar to that of many small disulfide-linked protein families, including the peptide toxins (19), we hypothesized that toxin peptides also could be grafted into CDR3H of the antibody scaffold. Here we demonstrate that selective Kv1.3 channel inhibitors Moka1-toxin and Vm24-toxin can be fused to human antibody scaffolds to generate antibody antagonists for the human Kv1.3 channel. Our data show that the Synagis (Syn)-Vm24-CDR3L fusion protein exhibited excellent in vitro and in vivo activity, as well as antibody-like pharmacologic properties.

Results and Discussion

Generation and Characterization of Antibody–Toxin CDR Fusions. For our initial antibody-toxin fusion protein constructs, we chose the humanized anti-lysozyme antibody HuLys (BVK), which has high structural similarity to the bovine antibody BLV1H12 (24). An engineered peptide, Moka1, derived from a scorpion toxin, has been reported to bind tightly and selectively to the Kv1.3 channel ($K_d = 1$ nM; >1,000-fold selectivity over Kv1.1 and KCa1.1) (28). We grafted this 34-aa, three disulfide-bonded peptide into the BVK scaffold to replace Ala93-Tyr102 in CDR3H using a β-strand stalk (Fig. 1). The resulting fusion construct, BVK-Moka1-CDR3H, was expressed in mammalian HEK293F cells by transient transfection, with a yield of 14 mg/L after purification. SDS/PAGE analysis revealed that the protein had >95% purity and migrated as a single band at a molecular mass of ~160 kDa (*SI Appendix*, Fig. S1). After reduction by DTT, the light chains migrated at ~25 kDa, whereas the heavy chains migrated at ~55–60 kDa, matching the calculated molecular mass. The identity was further confirmed by electrospray ionization (ESI)-mass spectrometry (MS) (*SI Appendix*, Fig. S2).

To test the generality of this approach, we next attempted to graft Moka1 into the CDR3H of the humanized antibody Syn, a Food and Drug Administration-approved respiratory syncytial virus (RSV)-neutralizing antibody. Syn has been used clinically to treat RSV infection in children since 1998. It does not bind any human proteins, and thus is an ideal carrier scaffold for fusion constructs (29, 30). All fusion antibodies were "Fc-null," carrying the human IgG1 heavy chain constant region with mutations (E233P, L234V, L235A, ΔG236, A327G, A330S, and P331S) to reduce complement-dependent cytotoxicity (CDC) and antibody-dependent cell-mediated cytotoxicity (ADCC) (27) (*SI Appendix*, Figs. S3 and S4). Unfortunately, the CDR3H fusion antibody was poorly expressed (<0.5 mg/L), suggesting a problem with proper folding or protein instability. Compared with the BVK scaffold, CDR3H of Syn is less solvent-exposed and might not sterically accommodate insertions as readily. Examination of the X-ray crystal structure (Fig. 1) suggested that CDR3L and CDR2H exhibit similar β-strand conformations with multiple intraloop hydrogen bonds but are more solvent-exposed, and thus may be better sites for the fusion of peptides. However, fusion of Moka1 to these CDRs with an antiparallel β-strand stalk also resulted in unsatisfactory protein yields, suggesting that either interloop interactions or interactions with surrounding CDRs (CDR2L, CDR3H, and CDR1H) do not favor the β-strand stalk.

As an alternative, we generated fusions using the previously reported coiled-coil linker (21). The Syn-Moka1 fusion protein was created by replacing either Gly92-Tyr93 in CDR3L or Asp56-Asp57 in CDR2H of Syn with the Moka1 sequence connected by a coiled-coil stalk to generate Syn-Moka1-CDR3L or Syn-Moka1-CDR2H, respectively (Fig. 1). These Syn-Moka1 fusion antibodies were transiently expressed in HEK293F cells, with a yield of 15.0 mg/L for Syn-Moka1-CDR3L and a yield of 2.5 mg/L for Syn-Moka1-CDR2H. SDS/PAGE analysis revealed > 90% purity (*SI Appendix*, Fig. S1). After reduction by DTT, the light chains migrated at 25–35 kDa and the heavy chains migrated at 50–65 kDa, matching the calculated molecular mass of peptide-fused and
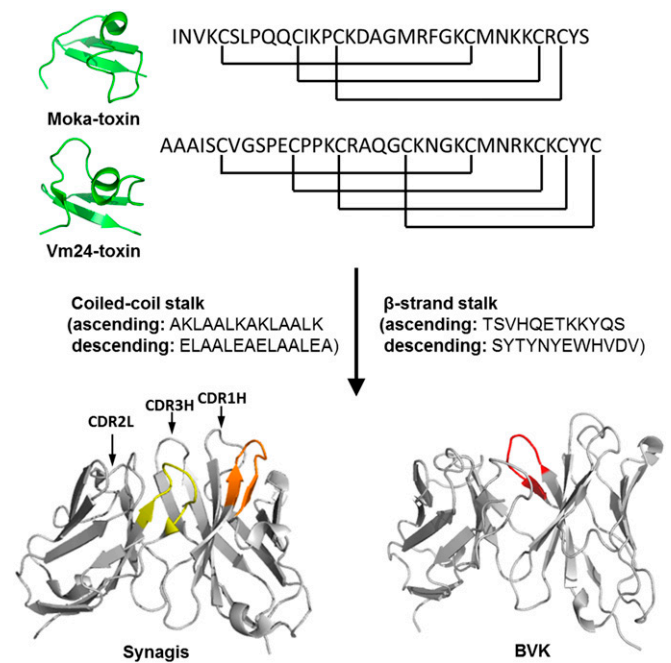

Fig. 1. Design of humanized anti-Kv1.3 antibodies. Solution NMR structures (green) of Moka1-toxin (PDB ID code: 2KIR) and Vm24-toxin peptides (PDB ID code: 2K9O) are shown with the corresponding sequences (disulfide bonds are indicated). Peptides were grafted into CDR3L (yellow) and CDR2H (orange) of Syn antibody (Fab fragment X-ray crystal structure depicted; PDB ID code: 2HWZ) or into CDR3H (red) of BVK antibody (Fab fragment depicted; PDB ID code: 1BVK).

nonfused heavy and light chains. Their identities were further confirmed by ESI-MS (*SI Appendix*, Fig. S5). The increased yields of the coiled-coil fusion proteins suggest that the linker design plays a critical role in the creation of viable CDR fusions. In addition, it also appears that different CDRs are able to accommodate insertions to different degrees.

We next assessed the biological activity of these fusion antibodies. First, to verify functional inhibition of Kv1.3, we acquired CHO cells stably expressing the human Kv1.3 channel and subjected them to the FluxOR potassium (K^+) channel assay. The IC_{50} for Syn-Moka1-CDR3L was determined to be 43.91 nM (*SI Appendix*, Fig. S6). Second, to demonstrate inhibitory function on the target cell type, we used primary T cells, activated by anti-CD3, to evaluate the effect of Kv1.3 blockade by peptide inhibitors, an established precedent in the field (30–32). T_{EM} cells can be selectively activated by αCD3-mediated T-cell receptor (TCR) signaling independent of costimulation, whereas full activation of naive T cells and T_{CM} cells requires costimulatory signals provided by CD28 and/or other protein members (3, 4, 33, 34). Thus, inhibition of the activation of T cells stimulated solely by αCD3 provides a straightforward method to assess the effect of Kv1.3 inhibitors on T_{EM} cells. T cells express CD69 during early stimulation, and gradually express CD25 as activation continues into the middle and late stages. Inflammatory cytokines, including TNF-α, are also secreted to promote T-cell proliferation and activate other immune cells (26).

Flow cytometry analysis and ELISAs (*SI Appendix*, Fig. S7 *A–D*) showed that the fusion antibodies can potently suppress T-cell activation. The most potent fusions were Syn-Moka1-CDR3L ($EC_{50} = 20.0 \pm 9.8$ nM for CD69, 8.4 ± 3.4 nM for CD25, 42.6 ± 10.6 nM for TNF-α, and 12.8 ± 6.5 nM for cell proliferation) and BVK-Moka1-CDR3H ($EC_{50} = 8.8 \pm 2.4$ nM for CD69, 10.9 ± 5.0 nM for CD25, 37.4 ± 10.6 nM for TNF-α, and 10.4 ± 4.5 nM for cell proliferation) (Table 1). We also assessed the viability of T cells in a 6-d proliferation assay, in which none of the antibody fusions showed significant cytotoxicity. These results suggest that

Table 1. Suppression of human T-cell activation by Moka1 and Vm24 peptide/fusion proteins

Construct	Fc	Yield, mg/L	EC_{50}, nM CD69	CD25	TNF-α	Proliferation
Moka1 peptide/fusion proteins						
Moka1-toxin			186.8 ± 46.6	27.8 ± 11.1	26.7 ± 10.1	24.4 ± 6.3
Syn-Moka1-CDR3L	Null	15.0	20.0 ± 9.8	8.4 ± 3.4	42.6 ± 10.6	12.8 ± 6.5
Syn-Moka1-CDR2H	Null	2.5	28.5 ± 10.4	3.2 ± 2.0	24.8 ± 15.6	15.1 ± 4.4
BVK-Moka1-CDR3H	Null	13.9	8.8 ± 2.4	10.9 ± 5.0	37.4 ± 10.6	10.4 ± 4.5
Moka1 and Vm24 peptide/fusion proteins						
Moka1-toxin				52.8 ± 28.3	19.7 ± 9.8	
Vm24-toxin				1.5 ± 0.8	0.02 ± 0.01	
Syn-Vm24-CDR3L	Null	18.3		0.4 ± 0.3	0.05 ± 0.03	
BVK-Vm24-CDR3H	Null	10.7		2.7 ± 1.6	0.2 ± 0.09	

CDR3H of BVK and CDR3L of Syn are suitable sites for the engraftment of toxin peptides.

Encouraged by these results with Moka1-toxin fusion, we next examined fusion of a more potent toxin, Vm24, a natural peptide identified from the venom of a Mexican scorpion. This 36-mer peptide consists of α-helix and β-strands, stabilized by four pairs of disulfide bonds (35). It has a K_d ~3 pM for Kv1.3 and >1,500-fold selectivity over Kv1.1, Kv1.2, KCa1.1, and KCa3.1 (36). Given that CDR3L was identified as a viable site for Moka1 fusion on Syn, we also used it to graft the Vm24-toxin peptide. For comparison, we also generated the Vm24 fusion to CDR3H of the BVK scaffold. Both antibodies were expressed in HEK293F cells with good yields (18.3 mg/L for Syn-Vm24-CDR3L and 10.7 mg/L for BVK-Vm24-CDR3H), and were characterized by SDS/PAGE and ESI-MS analysis to confirm their identities and purities (*SI Appendix,* Figs. S1 and S8). Syn-Vm24-CDR3L was first tested and appeared to be potent in the aforementioned K+ flux assay (IC_{50} = 0.59 nM) (*SI Appendix,* Fig. S6). Similar to the parent peptides, the Vm24 fusion antibodies were found to be more potent than Moka1-fusions in the inhibition of primary human T-cell activation (Table 1 and *SI Appendix,* Fig. S7). The Syn-Vm24-CDR3L fusion (EC_{50} = 0.4 ± 0.3 nM for CD25 expression and 0.05 ± 0.03 nM for TNF-α secretion) had greater activity than the BVK fusion (EC_{50} = 2.7 ± 1.6 nM for CD25 and 0.2 ± 0.09 nM for TNF-α), suggesting that the CDRs surrounding the fusion site or the stalk linkers affect the interaction between the toxin and Kv1.3 channel. Viability assays confirmed that the suppression of T-cell activation by Vm24 fusion antibodies was not due to cytotoxicity (*SI Appendix,* Fig. S9). Taken together, these results demonstrate excellent tolerance of selected CDRs to substitution by disulfide bond-rich peptides.

To further assess the activity and selectivity of the four most promising CDR fusions (Vm24/Moka1 fusion in Syn-CDR3L and BVK-CDR3H), we determined whether they can preferentially suppress the activation of T_{EM} cells. CCR7 T_{EM} cells were isolated from human peripheral blood T cells by removing the CCR7+ naive T cells and T_{CM} cells with biotinylated anti-CCR7 antibody using anti-biotin magnetic beads (37). Flow cytometry confirmed the T_{EM} cell fraction as 97.5% for CCR7− and 99.7% for CD3+ (*SI Appendix,* Fig. S10). After stimulation by αCD3 antibody, treatment with increasing concentrations of fusion antibodies inhibited the activation of human T_{EM} cells in a concentration-dependent manner (*SI Appendix,* Fig. S11 *A and B*), with Syn-Vm24-CDR3L the most potent fusion construct (EC_{50} = 0.91 ± 0.48 nM for CD25 expression and <0.048 nM for TNF secretion) (Table 2). Consistent with the results in the human T-cell assays, Syn-Vm24-CDR3L was more potent than its counterpart BVK-Vm24-CDR3H (EC_{50} = 2.40 ± 2.0 nM for CD25 and 0.27 ± 0.16 nM for TNF-α). Neither Syn nor BVK parent antibodies showed any activity, indicating that the observed immunosuppressive effects are due to the fused peptides.

For comparison, we also stimulated peripheral blood mononuclear cells (PBMCs) with αCD3 to assess the activation mediated largely by naive T cells and T_{CM} cells (*SI Appendix,* Fig. S11 *C and D*) (37, 38). FK506, a nonspecific immunosuppressant, served as a control. As expected, FK506 effectively suppressed the activation of PBMCs (EC_{50} = 0.58 ± 0.33 nM for CD25 and 0.14 ± 0.09 nM for TNF-α) and showed no selectivity between T_{EM} and T_{CM} + naive T-cell populations. In contrast, Vm24 peptide and Vm24 antibody fusions, especially Syn-Vm24-CDR3L, were highly selective against T_{EM} cells, likely due to the high selectivity for Kv1.3 over KCa3.1 (>1,500 fold for Vm24) (30) (Table 2). In contrast, Moka1 peptide and Moka1 antibody fusions were less selective against T_{EM}.

Because the toxin peptides have nonhuman sequences, immunogenicity is a potential risk in developing these molecules as therapies that will be chronically administered to humans. As an initial assessment, an in silico immunogenicity evaluation was performed (EpiVax), which indicated that Syn-Vm24-CDR3L has favorably low immunogenicity potential in the range of the scores of the therapeutic antibodies with low immunogenicity in the clinic.

Table 2. Selectivity of Moka1 and Vm24 peptide/fusion proteins on human T_{EM} cells

Construct	Fc	EC_{50} (nM) on T_{EM} cells CD25	TNF-α	EC_{50} (nM) on PBMCs CD25	TNF-α
FK506		2.31 ± 1.20	0.66 ± 0.26	0.58 ± 0.33	0.14 ± 0.09
Moka1-toxin		115.7 ± 52.4	135.3 ± 52.2	175.9 ± 110	>200
Vm24-toxin		0.73 ± 0.54	<0.048	>200	>200
Syn-Moka1-CDR3L	Null	104.6 ± 53.9	33.6 ± 18.0	79.9 ± 36.0	>200
BVK-Moka1-CDR3H	Null	147.9 ± 66.7	51.2 ± 28.1	111.5 ± 55.7	>200
Syn-Vm24-CDR3L	Null	0.91 ± 0.48	<0.048	>200	>200
BVK-VM24-CDR3H	Null	2.40 ± 2.0	0.27 ± 0.16	96.6 ± 45.8	>200
Syn	Null	>200	>200		
BVK	Null	>200	>200		

www.manaraa.com

Serum Stability and Pharmacokinetic Analysis of Syn-Vm24-CDR3L Fusion. Given that the Vm24 antibody fusion showed the most potent activity in vitro, we next examined its stability in freshly collected rat serum for up to 72 h (*SI Appendix*, Fig. S12). The amount of Syn-Vm24-CDR3L was determined by ELISA based on quantitation of the Vm24 antibody fusion that is able to bind Kv1.3. After 72 h of incubation, 52% of the Vm24 peptide remained, compared with 84% of Syn-Vm24-CDR3L.

We next performed a pharmacokinetic (PK) analysis of Syn-Vm24-CDR3L in rats, analyzing plasma samples using the same ELISA method described above. Syn-Vm24-CDR3L had a long half-life, with estimated terminal half-lives of 54.0 h for intravenous injection (*SI Appendix*, Fig. S13) and 38.4 h for subcutaneous injection (Fig. 2*A*), much longer than those reported for ShK-186 (<10 min in rats), the most advanced Kv1.3 inhibitor in development (18).

In Vivo Efficacy of Syn-Vm24-CDR3L Fusion. We evaluated Syn-Vm24-CDR3L in vivo for its effectiveness in suppressing delayed-type hypersensitivity (DTH) in rats, a response regulated mainly by the activation of CD4$^+$ T$_{EM}$ cells in the skin (18). Lewis rats were immunized with ovalbumin on the first day, and then challenged again with ovalbumin injection into the left ear after 1 wk of sensitization. The challenged ear was swollen, and ear thickness was measured after 24 h as an indication of the immune response against ovalbumin. Because Syn-Vm24-CDR3L reached its maximum concentration at ~24 h, it was administered subcutaneously 1 d before the ovalbumin challenge as a single dose or 2 d before the challenge as two consecutive daily injections of 5 mg/kg/dose (equal to 28 nmol/kg/dose). Owing to their short half-lives, the ShK and Vm24 peptides were administered subcutaneously 1 d later than the antibody at 100 μg/kg/dose (equal to 25 nmol/kg/dose). As shown in Fig. 2*B*, all peptides and antibody fusions showed dose-responsive inhibition of the DTH. Syn-Vm24-CDR3L effectively reduced the change in ear thickness (~0.3 mm) by 28% after one injection and by 38% after two doses. Vm24 peptide also showed activity in this experiment, albeit to a lesser extent (15% reduction of the difference in ear thickness with one dose, 27% reduction with two doses). Notably, in this dosing paradigm, the in vivo activity of Syn-Vm24-CDR3L is close to that of the parent ShK peptide (34% reduction of the difference in ear thickness with one dose and 43% reduction with two doses). Future in vivo studies using different dosing frequencies and dosages are planned to gain a better understanding of the PK/pharmacodynamics relationship of Syn-Vm24-CDR3L.

Conclusion

In summary, we have demonstrated the versatility of the antibody-CDR loop fusion strategy by generating a specific antibody inhibitor of the human Kv1.3 channel. The fusion of toxins into CDR3L of Syn via a coiled-coil linker exhibited superior activity to other fusions. The antibody-toxin fusion showed excellent in vitro potency and selectivity in assays with human T$_{EM}$ cells. Syn-Vm24-CDR3L also significantly suppressed the DTH reactions in vivo in rats. Based on the role of T$_{EM}$ in human autoimmune diseases, future studies will explore the efficacy of the antibody toxin fusion in disease models in support of human testing in multiple sclerosis, inflammatory bowel disease, type 1 diabetes, psoriasis, and systemic lupus erythematosus.

Materials and Methods

Peptide Synthesis. Moka1 and Vm24 toxin peptides were synthesized in solid phase by InnoPep. Peptide folding, HPLC purification, and LC-MS validation were performed based on previously published procedures (28, 35).

Cloning of Antibody Expression Vector. The genes encoding Moka1 and Vm24 were synthesized by Integrated DNA Technologies (IDT) and amplified by PCR using PfuUltra II DNA polymerase (Agilent). The DNA sequences of Moka1 and Vm24 peptides are ATCAACGTGAAGTGCAGCCTGCCCCAGCAGTGCA-TCAAGCCCTGCAAGGACGCCGGCATGCGGTTCGGCAAGTGCATGAACAAGAA-GTGCAGGTGCTACAGC and GCCGCTGCAATCTCCTGCGTCGGCAGCCCCGA-
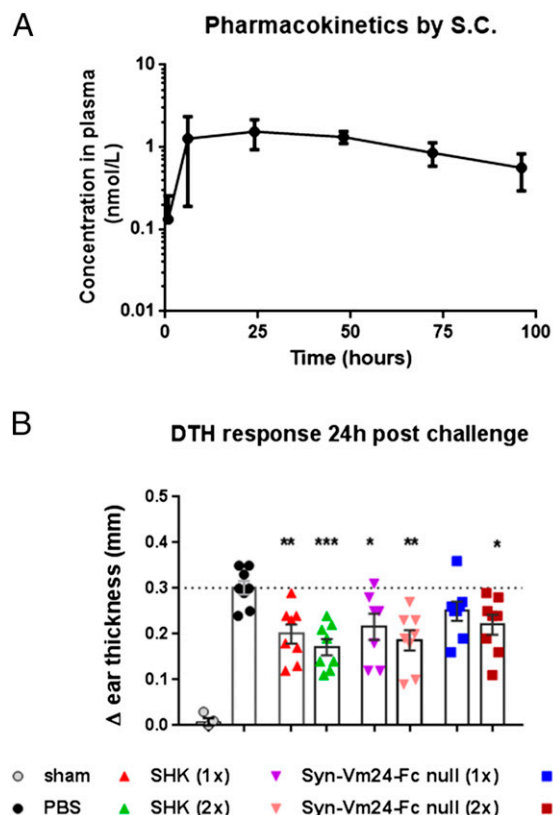

Fig. 2. In vivo pharmacologic performance of Syn-Vm24-CDR3L. (*A*) PK was evaluated at a single dose of 2 mg/kg via subcutaneous injection. (*B*) In vivo inhibition of the DTH reaction in rats (*n* = 8 per group) following subcutaneous administration of Syn-Vm24-CDR3L (5 mg/kg), ShK peptide (100 μg/kg), Vm24 peptide (100 μg/kg), and PBS vehicle groups. All treatment groups were challenged in the left ear with 1 mg/mL ovalbumin/complete Freund's adjuvant on day 7, except for the sham group, in which both ears were injected with PBS. Peptides were injected with a single dose on the day of challenge (1×) or at one daily dose starting 24 h before the challenge (2×). Syn-Vm24-CDR3L was injected with a single dose at 24 h before the challenge (1×) or at one daily dose starting 48 h before the challenge (2×). Shown are the ear thickness differences between the left and right ears at 24 h after ovalbumin challenge.

ATGTCCTCCCAAGTGCCGGGCTCAGGGATGCAAGAACGGCAAGTGTATGA-ACCGGAAGTGCAAGTGCTACTATTGC, respectively. The DNA fragments encoding the heavy chains and light chains of Syn and BVK, along with the linkers (coiled-coil or β-strand) (24, 27) were also synthesized by IDT and amplified by PCR. The fusion gene fragments were assembled by overlap extension PCR and digested with the restriction enzymes EcoRI-HF and NheI-HF (New England Biolabs), followed by DNA gel extraction. The final expression vectors for the fusion antibodies were constructed by in-frame ligation of the assembled DNA into the pFuse backbone (Invivogen) using T4 DNA ligase. The sequences of the resulting mammalian expression vectors were confirmed by DNA sequencing (GENEWIZ).

Expression and Purification of the Antibody Fusion Proteins. The genes containing the heavy chains and light chains of the antibody fusions were coexpressed by transient transfection in HEK 293F cells (Life Technologies). The HEK 293F cells were cultured in shaker flasks containing FreeStyle medium (Life Technologies), and were shaken at 125 rpm at 37 °C, with 5% CO$_2$. For transfection, HEK 293F cells were grown up to a density of 1 million cells/mL and were transfected with the light chain plasmid, heavy chain plasmid, and 293F at a ratio of 1:2:6 following the manufacturer's instructions. The expression media were harvested and sterile-filtered twice every 48 h after transfection to collect the secreted proteins. The fusion antibodies were purified by Protein A chromatography (Thermo Fisher Scientific) and analyzed by SDS/PAGE and MS analysis.

Labeling of Antibody Fusions with Alexa Fluor 488. Alexa Fluor 488-NHS ester (50 nmol in 5 μL DMSO; Life Technologies) was added to the solution of

www.manaraa.com

BVK-Moka1-CDR3H (Fc null mutant or Fc; 0.5 mg, 3.3 nmol) in PBS buffer (500 μL, pH 7.4). The mixture was stirred at 25 °C for 2 h with shaking at 50 rpm, and then purified by FPLC with a size-exclusion column (Superdex 200 10/300 GL; GE Healthcare). Alternatively, the mixture could be quickly purified by excess buffer exchange with an Amicon filter (30-kDa molecular mass cutoff; EMD Millipore) or Zeba spin desalting columns (7-kDa molecular mass cutoff; Thermo Fisher Scientific). The extent of labeling—drug-to-antibody ratio (DAR)—was characterized by ESI-Q-TOF protein MS. The results are shown in *SI Appendix*, Fig. S3.

Confirmation of Fc Null Caused by Seven-Point Mutations. To confirm that the seven point mutations in Fc of the antibody fusions can significantly reduce the undesired ADCC and CDC effects mediated by Fcγ receptor interactions, BVK-Moka1-CDR3H (Fc null) with mutated Fc and WT Fc labeled with Alexa Fluor 488 were incubated with THP-1, a human monocytic cell line with high Fcγ receptor expression. BVK-Moka1-CDR3H did not bind to THP-1 at concentrations up to 100 nM, whereas BVK-Moka1-CDR3H with WT Fc bound significantly to THP-1 at concentrations as low as 1 nM (*SI Appendix*, Fig. S4).

Potassium FluxOR Assay. CHO cells stably expressing human Kv1.3 were acquired from B'SYS-Mayflower Biosciences and cultured in DMEM/Ham's F-12 Nutrient Mixture [with 10% (vol/vol) FBS, 100 IU/mL penicillin, 100 μg/mL streptomycin, and 100 μg/mL hygromycin B] and plated at 5×10^4 cells per well in 384-well plates. The FluxOR potassium channel assay was performed as specified by the manufacturer (Thermo Fisher Scientific) and imaged using the Molecular Devices FLIPR platform. After cell attachment overnight, the medium was decanted, and loading buffer was added and incubated for 1 h at room temperature. The peptides or fusions were serially diluted in FluxOR assay buffer. The loading buffer was decanted from the cells, and the assay buffer containing peptides or fusions were added, followed by incubation for an additional 45 min at room temperature. The cells were stimulated with 5 mM K_2SO_4 in stimulation buffer. After reading on FLIPR, the difference of maximum and minimum fluorescent intensities over a 3-min read was calculated for each well.

Flow Cytometry Analysis. Surface antigen expression analysis was performed using the following fluorophore-conjugated anti-human antibodies: αCD3-PB (UCHT1; BioLegend), αCD69-PE (FN50; BioLegend), αCD25-APC/Cy7 (M-A251; BioLegend), αCD45RA-PB (HI100; BioLegend), and αCCR7-Alexa Fluor 647 (3D12; BD Pharmingen). Human T cells or T_{EM} cells were stained with these antibodies in HBSS (Mediatech)/2% (vol/vol) FBS for 60 min at 4 °C, then washed twice with the same medium and analyzed on an LSR II flow cytometer equipped with a high-throughput sampler (BD Bioscience). For Fc blocking, human TruStain FcX (BioLegend) was added, followed by a 20-min incubation before staining with other antibodies of interest. All results were processed with FlowJo software.

Human T Cell Activation. Human T-cell activation was performed based on published procedures (26, 30–32). In brief, T cells were isolated from freshly purified PBMCs using a T-cell–negative enrichment kit (StemCell Technologies). The purity was >95% based on CD3$^+$ signals monitored by flow cytometry. The freshly isolated T cells were suspended in RPMI medium [with 10% (vol/vol) FBS, 100 IU/mL penicillin, and 100 μg/mL streptomycin] and plated at 1.5×10^5 cells per well in flat-bottom 96-well plates. Proteins and peptides were serially

diluted in PBS as 10× stock and added in triplicate to T cells, respectively. After a 1-h preincubation, the samples were transferred to a new plate coated with 1 μg/mL OKT3 (eBioscience) and then incubated at 37 °C in 5% CO₂ for 72 h, after which the secreted supernatants were collected for TNF-α analysis. The cytokine level was measured by ELISA using the DuoSet development kit (R&D Systems), and the results were processed with GraphPad Prism. T-cell antigen marker CD25 was analyzed by flow cytometry using the procedure described above. With another separate set of samples, T-cell antigen marker CD69 was analyzed at ~24 h after stimulation. For the proliferation assay, purified T cells were labeled with 2 μM carboxyfluorescein succinimidyl ester (Thermo Fisher Scientific) based on the manufacturer's instructions, followed by incubation with peptide/protein samples and activation by αCD3. The mixtures were incubated for 6 d, followed by washing with HBSS/2% (vol/vol) FBS and flow cytometry analysis on the FITC channel.

Human T_{EM} Cell Activation Assay. Human T_{EM} cells were isolated following published procedures (37). In general, purified T cells were suspended at a concentration of 10⁷ cells/50 μL of RoboSep buffer (StemCell Technologies) and incubated with a biotinylated anti-CCR7 antibody (3D12; BD PharMingen) at a ratio of 20 of μL antibody per 1 million cells. The mixture was incubated at room temperature for 15 min, followed by washing with at least 2 mL of buffer per 10⁷ cells. The labeled cells were resuspended in RoboSep buffer and then mixed with anti-biotin MicroBeads (Miltenyi Biotec) at a ratio of 20 μL of antibody per 10 million cells. The mixture was incubated at room temperature for 10 min, washed once, resuspended in 500 μL of buffer, and loaded onto an LD Column (Miltenyi Biotec) for a negative selection aided by Magnet. The eluted cells were pure T_{EM} cells, which were then seeded at 50,000 cells per well, treated, activated, and characterized using the aforementioned procedures described for human T-cell activation.

Cell Cytotoxicity Studies. After aspiration of supernatant, the cell mixture was resuspended, with 50 μL of the 150-μL cell culture volume pipetted out from each sample well and transferred into a new plate. Cell viability was measured by quantifying the ATP content with CellTiter-Glo (Promega), for which the luminescence was detected on a Gemini EM microplate reader (Molecular Devices). The viability of unstimulated T cells, defined as 100%, served as a control.

In Vitro Selectivity Studies. To determine the effect of peptide/protein samples on naive T cells and T_{CM} cells, human PBMCs were freshly prepared and seeded at 200,000 cells per well. After preincubation with increasing concentrations of samples for 1 h, the cell mixtures were stimulated by 500 ng/mL soluble OKT3 for 24 h. The follow-up characterizations were the same as those described for human T-cell/T_{EM} cell activation. The only difference is that for flow cytometry analysis, cells were also stained with αCD3 to allow for specific gating on T cells.

All animals and pharmacology studies were in accordance with National Institute of Health guidelines and were approved by the Institutional Animal Care and Use Committee (California Institute of Biomedical Research). Detailed descriptions of methods and materials are in *SI Appendix, Materials and Methods*.

1. Wulff H, et al. (2003) The voltage-gated Kv1.3 K(+) channel in effector memory T cells as new target for MS. *J Clin Invest* 111(11):1703–1713.
2. Ellis CN, Krueger GG; Alefacept Clinical Study Group (2001) Treatment of chronic plaque psoriasis by selective targeting of memory effector T lymphocytes. *N Engl J Med* 345(4):248–255.
3. Fasth AE, Cao D, van Vollenhoven R, Trollmo C, Malmström V (2004) CD28^{null}CD4$^+$ T cells: Characterization of an effector memory T-cell population in patients with rheumatoid arthritis. *Scand J Immunol* 60(1-2):199–208.
4. Markovic-Plese S, Cortese I, Wandinger KP, McFarland HF, Martin R (2001) CD4$^+$CD28$^-$ costimulation-independent T cells in multiple sclerosis. *J Clin Invest* 108(8):1185–1194.
5. Viglietta V, Kent SC, Orban T, Hafler DA (2002) GAD65-reactive T cells are activated in patients with autoimmune type 1a diabetes. *J Clin Invest* 109(7):895–903.
6. Grishkan IV, Ntranos A, Calabresi PA, Gocke AR (2013) Helper T cells down-regulate CD4 expression upon chronic stimulation giving rise to double-negative T cells. *Cell Immunol* 284(1-2):68–74.
7. Nicolaou SA, et al. (2010) Differential calcium signaling and Kv1.3 trafficking to the immunological synapse in systemic lupus erythematosus. *Cell Calcium* 47(1):19–28.
8. Nicolaou SA, et al. (2007) Altered dynamics of Kv1.3 channel compartmentalization in the immunological synapse in systemic lupus erythematosus. *J Immunol* 179(1):346–356.
9. Poulopoulou C, et al. (2008) Glutamate levels and activity of the T cell voltage-gated potassium Kv1.3 channel in patients with systemic lupus erythematosus. *Arthritis Rheum* 58(5):1445–1450.
10. Yoon KH (2010) Efficacy and cytokine modulating effects of tacrolimus in systemic lupus erythematosus: A review. *J Biomed Biotechnol* 2010:686480.
11. Kahan BD (1993) Cyclosporine: The base for immunosuppressive therapy—present and future. *Transplant Proc* 25(1 Pt 1):508–510.
12. Coutinho AE, Chapman KE (2011) The anti-inflammatory and immunosuppressive effects of glucocorticoids, recent developments and mechanistic insights. *Mol Cell Endocrinol* 335(1):2–13.
13. Tung TH (2010) Tacrolimus (FK506): Safety and applications in reconstructive surgery. *Hand (NY)* 5(1):1–8.
14. Stanbury RM, Graham EM (1998) Systemic corticosteroid therapy: Side effects and their management. *Br J Ophthalmol* 82(6):704–708.
15. Azam P, Sankaranarayanan A, Homerick D, Griffey S, Wulff H (2007) Targeting effector memory T cells with the small molecule Kv1.3 blocker PAP-1 suppresses allergic contact dermatitis. *J Invest Dermatol* 127(6):1419–1429.
16. Chandy KG, et al. (2004) K$^+$ channels as targets for specific immunomodulation. *Trends Pharmacol Sci* 25(5):280–289.
17. Beeton C, et al. (2006) Kv1.3 channels are a therapeutic target for T cell-mediated autoimmune diseases. *Proc Natl Acad Sci USA* 103(46):17414–17419.
18. Tarcha EJ, et al. (2012) Durable pharmacological responses from the peptide ShK-186, a specific Kv1.3 channel inhibitor that suppresses T cell mediators of autoimmune disease. *J Pharmacol Exp Ther* 342(3):642–653.
19. Wang F, et al. (2013) Reshaping antibody diversity. *Cell* 153(6):1379–1393.

Wang et al.

APPLIED BIOLOGICAL SCIENCES

20. Liu T, et al. (2014) Rational design of CXCR4-specific antibodies with elongated CDRs. *J Am Chem Soc* 136(30):10557–10560.

21. Zhang Y, et al. (2014) An antibody with a variable-region coiled-coil "knob" domain. *Angew Chem Int Ed Engl* 53(1):132–135.

22. Zhang Y, et al. (2013) Functional antibody CDR3 fusion proteins with enhanced pharmacological properties. *Angew Chem Int Ed Engl* 52(32):8295–8298.

23. Zhang Y, et al. (2013) An antibody CDR3-erythropoietin fusion protein. *ACS Chem Biol* 8(10):2117–2121.

24. Liu T, et al. (2015) Rational design of antibody protease inhibitors. *J Am Chem Soc* 137(12):4042–4045.

25. Liu T, et al. (2015) Functional human antibody CDR fusions as long-acting therapeutic endocrine agonists. *Proc Natl Acad Sci USA* 112(5):1356–1361.

26. Wang RE, et al. (2015) An immunosuppressive antibody-drug conjugate. *J Am Chem Soc* 137(9):3229–3232.

27. Zhang Y, et al. (2015) Rational design of a humanized glucagon-like peptide-1 receptor agonist antibody. *Angew Chem Int Ed Engl* 54(7):2126–2130.

28. Takacs Z, et al. (2009) A designer ligand specific for Kv1.3 channels from a scorpion neurotoxin-based library. *Proc Natl Acad Sci USA* 106(52):22211–22216.

29. American Academy of Pediatrics Committee on Infectious Diseases; American Academy of Pediatrics Bronchiolitis Guidelines Committee (2014) Updated guidance for palivizumab prophylaxis among infants and young children at increased risk of hospitalization for respiratory syncytial virus infection. *Pediatrics* 134(2):415–420. Erratum in *Pediatrics* 134(6):1221.

30. Hu L, et al. (2013) Blockade of Kv1.3 potassium channels inhibits differentiation and granzyme B secretion of human CD8^{+} T effector memory lymphocytes. *PLoS One* 8(1): e54267.

31. Kalman K, et al. (1998) ShK-Dap22, a potent Kv1.3-specific immunosuppressive polypeptide. *J Biol Chem* 273(49):32697–32707.

32. Middleton RE, et al. (2003) Substitution of a single residue in *Stichodactyla helianthus* peptide, ShK-Dap22, reveals a novel pharmacological profile. *Biochemistry* 42(46): 13698–13707.

33. Croft M, Bradley LM, Swain SL (1994) Naive versus memory CD4 T cell response to antigen: Memory cells are less dependent on accessory cell costimulation and can respond to many antigen-presenting cell types including resting B cells. *J Immunol* 152(6):2675–2685.

34. Boesteanu AC, Katsikis PD (2009) Memory T cells need CD28 costimulation to remember. *Semin Immunol* 21(2):69–77.

35. Gurrola GB, et al. (2012) Structure, function, and chemical synthesis of *Vaejovis mexicanus* peptide 24: A novel potent blocker of Kv1.3 potassium channels of human T lymphocytes. *Biochemistry* 51(19):4049–4061.

36. Varga Z, et al. (2012) Vm24, a natural immunosuppressive peptide, potently and selectively blocks Kv1.3 potassium channels of human T cells. *Mol Pharmacol* 82(3):372–382.

37. Schmitz A, et al. (2005) Design of PAP-1, a selective small molecule Kv1.3 blocker, for the suppression of effector memory T cells in autoimmune diseases. *Mol Pharmacol* 68(5):1254–1270.

38. Beeton C, et al. (2005) Targeting effector memory T cells with a selective peptide inhibitor of Kv1.3 channels for therapy of autoimmune diseases. *Mol Pharmacol* 67(4):1369–1381.

www.manaraa.com